

John W. McClintic¹

Walker Department of Mechanical Engineering,
The University of Texas at Austin,
204 E. Dean Keeton Street,
Austin, TX 78712
e-mail: johnwmclintic@gmail.com

Dale W. Fox²

Walker Department of Mechanical Engineering,
The University of Texas at Austin,
204 E. Dean Keeton Street,
Austin, TX 78712
e-mail: Dale.Fox@utexas.edu

Fraser B. Jones

Walker Department of Mechanical Engineering,
The University of Texas at Austin,
204 E. Dean Keeton Street,
Austin, TX 78712
e-mail: me.fbjones@gmail.com

David G. Bogard

Walker Department of Mechanical Engineering,
The University of Texas at Austin,
204 E. Dean Keeton Street,
Austin, TX 78712
e-mail: dbogard@mail.utexas.edu

Thomas E. Dyson

GE Global Research Center,
1 Research Circle,
Schenectady, NY 12309
e-mail: dyson@ge.com

Zachary D. Webster

GE Aviation,
1 Neumann Way,
Cincinnati, OH 45125
e-mail: Zachary.Webster@ge.com

Flow Physics of Diffused-Exit Film Cooling Holes Fed by Internal Crossflow

Internal crossflow, or internal flow that is perpendicular to the overflowing mainstream, reduces film cooling effectiveness by disrupting the diffusion of coolant at the exit of axial shaped holes. Previous experimental investigations have shown that internal crossflow causes the coolant to bias toward one side of the diffuser and that the severity of the biasing scales with the inlet velocity ratio, VR_i , or the ratio of crossflow velocity to the jet velocity in the metering section of the hole. It has been hypothesized and computationally predicted that internal crossflow produces an asymmetric swirling flow within the hole that causes the coolant to bias in the diffuser and that biasing contributes to ingestion of hot mainstream gas into the hole, which is undesirable. However, there are no experimental measurements as of yet to confirm these predictions. In the present study, in- and near-hole flow field and thermal field measurements were performed to investigate the flow structures and mainstream ingestion for a standard axial shaped hole fed by internal crossflow. Three different inlet velocity ratios of $VR_i = 0.24, 0.36$, and 0.71 were tested at varying injection rates. Measurements were made in planes normal to the nominal direction of coolant flow at the outlet plane of the hole and at two downstream locations— $x/d = 0$ and 5 . The predicted swirling structure was observed for the highest inlet velocity ratio and flow within the hole was shown to scale with VR_i . Ingestion within the diffuser was significant and also scaled with VR_i . Downstream flow and thermal fields showed that increased biasing contributed to more severe jet detachment and coolant dispersion away from the surface. [DOI: 10.1115/1.4042166]

Introduction

Gas Turbine Film Cooling. High turbine inlet temperatures in modern gas turbine engines necessitate active cooling of hot gas path components using cooler air drawn from the high pressure compressor. In early stage turbine blades, the coolant is delivered to the base of the blade from which it typically is passed through a series of internal channels and other features designed to maximize heat transfer between the coolant and the blade interior. The coolant is then exhausted as film cooling through discrete film cooling holes designed to spread the coolant onto the surface of the part. The efficiency with which the ejected coolant protects the part from the hot mainstream gas is the film cooling effectiveness, which is the normalized adiabatic wall temperature and defined as

$$\eta \equiv \frac{T_{\infty} - T_{aw}}{T_{\infty} - T_j} \quad (1)$$

Many factors contribute to η , a number of which are discussed in summary papers such as Refs. [1] and [2]. The focus of the present study is the impact of internal flow, specifically internal crossflow on the film cooling effectiveness of a standard laidback fan-shaped film cooling hole.

Internal Crossflow Effects. For the purposes of this study, the term “internal crossflow” will refer to an internal flow that is perpendicular to the overflowing mainstream air. A few studies have tested the impact of internal crossflow on diffused-exit or “shaped” film cooling holes [3–6]. Gritsch et al. [3] found that for fan-shaped and laidback fan-shaped holes, internal crossflow reduced film cooling effectiveness relative to holes fed by a quiescent plenum. The reduction in effectiveness occurred because the coolant biased toward one side of the diffuser, resulting in decreased lateral spreading of the jet. Two studies by Saumweber and Schulz [4,5] investigated crossflow effects further. In Ref. [4], a wider range of injection rates was tested for the fan-shaped holes of Ref. [3], and it was found that the direction and severity of biasing in the diffuser was dependent on both the internal crossflow velocity and the injection rate. In Ref. [5], the lateral diffusion angle, injection angle, and hole metering length were varied, and it was shown that each of these parameters also impacted the

¹Present address: Honeywell Aerospace, Phoenix, AZ 85034.

²Corresponding author.

Contributed by the International Gas Turbine Institute (IGTI) of ASME for publication in the JOURNAL OF TURBOMACHINERY. Manuscript received November 9, 2018; final manuscript received November 26, 2018; published online January 16, 2019. Editor: Kenneth Hall.

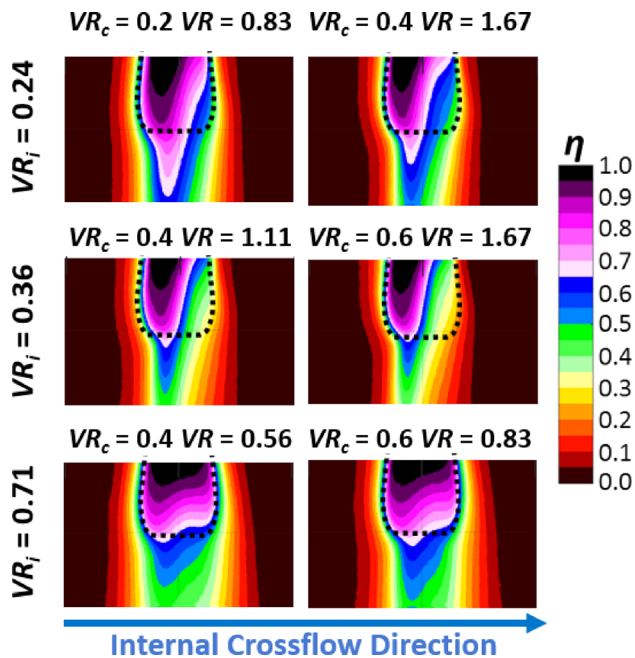


Fig. 1 Near-hole contours of η , measured in Ref. [6]

direction and severity of biasing within the diffuser and thus affected the film cooling effectiveness.

Recently, a study in this laboratory [6], tested a wide range of coolant-to-mainstream velocity ratios, VR_c , and injection rates for a standard laidback fan-shaped hole. That study showed that the direction and severity of biasing within the diffuser scaled with the ratio of the internal crossflow velocity to the mean velocity of the jet in the metering section of the hole or the inlet velocity ratio, VR_i . This result is demonstrated in Fig. 1, which shows contours of effectiveness within and immediately downstream of the hole with the diffuser breakout outlined. The near-hole contours were remarkably similar at matched VR_i . The biasing within the diffuser was most extreme at $VR_i = 0.36$ and started to reverse direction as it was increased to $VR_i = 0.71$. These measurements demonstrated the need for in- and near-hole velocity and thermal field measurements to study the important flow physics governing the performance of these conditions.

The film cooling data from previous studies suggest that the flow field within the crossflow-fed shaped hole differs substantially from that of a hole fed by a quiescent plenum. The experimental data of studies by Pietzryk et al. [7,8] and Issakhanian et al. [9] and computational efforts by Leylek and Zerkle [10] and Oliver et al. [11] show that for a plenum-fed hole, the flow separates on the downstream edge of the hole inlet, causing the bulk of the coolant to accelerate around the separation region. As shown in Ref. [11], a second separation can form as the flow enters the diffuser causing most of the coolant to exit from the upstream side of the hole. As the flow exits the diffuser, a pair of counter-rotating vortices are formed as the mainstream rolls over and around the issuing film cooling jet. This vortex pair was computationally predicted by Oliver et al. [11] and experimentally measured by Schroeder and Thole [12] for the same 7-7-7 standard laidback fan-shaped hole tested in this study and by McClintic et al. [6]. The counter-rotating vortex pair degrades film effectiveness by pulling mainstream air under the jet and transporting coolant away from the surface.

Previous computational studies have predicted the in-hole flow for shaped film cooling holes fed by internal crossflow to be substantially different than that of a plenum-fed hole. Saumweber and Schulz [4] predicted that the internal crossflow sets up an asymmetric swirl within the metering section of the hole. This swirling flow resulted in an asymmetric counter-rotating vortex

pair with a greater strength than that of the plenum-fed jet. The increased vortex strength caused the coolant to more rapidly disperse away from the wall for the crossflow case. A study by Kohli and Thole [13] also simulated crossflow-fed shaped holes with different internal crossflow velocities and hole metering lengths. That study also predicted an asymmetric swirl within the hole that strengthened with the increasing crossflow velocity. They further predicted that feeding the holes with an internal crossflow allowed hot mainstream air to ingest into the diffuser, warming the coolant before it exited the hole.

Present Study. The computational predictions of [4] and [13] provide insight into internal crossflow effects on film cooling that potentially explains previous experimental results. A swirling flow at the inlet of the hole could explain why the coolant biases at the inlet of the diffuser and why there exists an inlet velocity ratio at which the biasing is maximum before it reverses the direction. The vortical structures downstream of the film holes also likely contribute to an unfavorable dispersal of the coolant away from the surface. However, Reynolds-averaged Navier-Stokes simulations like those performed in Refs. [4] and [13] are notoriously poor at predicting film cooling performance. In this study, particle image velocimetry (PIV) was used to observe the flow structure within the diffuser and downstream of a 7-7-7 shaped film cooling hole to verify the previous computational predictions and to provide insight into the flow physics governing the crossflow effect. Furthermore, the temperature fields in and downstream of the hole were measured to study the impact of the injection rate and crossflow velocity on ingestion into the diffuser and dispersal of the jet downstream. The results of this study are intended to provide insight benefitting hot section film hole design and to provide a database for the validation of computational codes.

Experimental Facilities and Procedures

Description of Facilities. Experiments for this study were conducted in a low speed, low temperature recirculating wind tunnel facility at the University of Texas at Austin. A detailed description of the facility can be found in Anderson et al. [14] and Wilkes et al. [15]. The test section was configured for experimental film cooling on a flat plate as shown in Fig. 2. The test section afforded control over the approach flow turbulence intensity and boundary layer characteristics, which are shown in Table 1 alongside other relevant freestream parameters, all of which were held constant for all experiments in this study. These parameters were selected to match those of the previous study [6], that is measured film

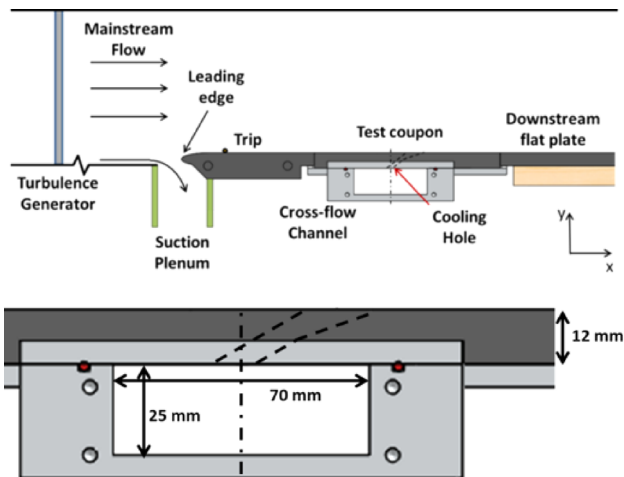
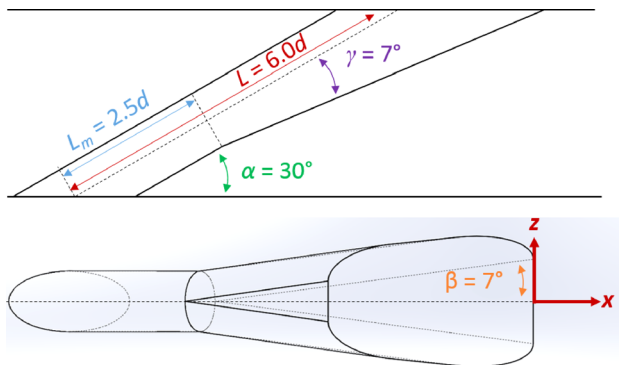


Fig. 2 Schematic of test section and channel

Table 1 Mainstream parameters

Parameter	Value
Cooling hole diameter (d)	4.0 mm
Mainstream temp (T_∞)	310 K
Mainstream velocity (U_∞)	25 m/s
Mainstream turbulence intensity (T_u)	4.8%
Turbulence integral length scale (Λ_u/d)	2.5
Approach boundary layer thickness (δ/d)	2.9
Boundary layer displacement thickness (δ^*/d)	0.36
Boundary layer momentum thickness (θ/d)	0.27
Boundary layer shape factor (H)	1.33
Approach Reynolds number ($Re_d = \rho_\infty U_\infty d / \mu$)	6000

**Fig. 3 7-7-7 film cooling hole geometry**

cooling effectiveness for the same geometry. These parameters are considered to be relevant to engine conditions.

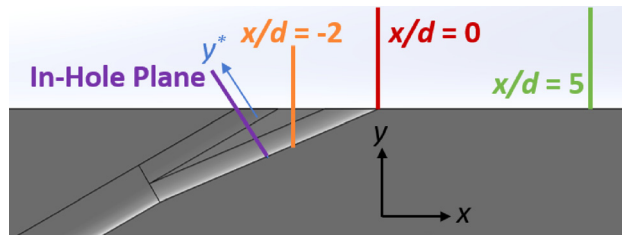
The film cooling holes were fed by a crossflow channel oriented perpendicular to the main flow loop as shown in Fig. 2. The channel flow was fully developed by the time it reached the film cooling holes. The test coupon was the same as used in Ref. [6] and had a single row of eight film cooling holes. The coupon was constructed from a closed cell polyurethane foam (General Plastics (Tacoma, WA) Last-a-Foam® R-3315) with a thermal conductivity of $k = 0.044$ W/m·K in order to minimize conduction errors. The film cooling holes were the standard 7-7-7 laidback fan-shaped film cooling holes first presented by Schroeder and Thole [16] and are diagrammed in Fig. 3.

The conditions tested in this study were selected from the test matrix for [6] and are shown in Table 2. Three inlet velocity ratios, VR_i , were chosen based on the results of Ref. [6]. $VR_i = 0.36$ corresponded to the maximum degree of biasing within the diffuser. The other two velocity ratios were chosen to bracket that maximum. Two different conditions were chosen for each inlet velocity ratio to determine sensitivity to injection rate at matched VR_i . Similarly, $VR = 0.83$ and 1.67 were tested at two different VR_i to show the impact of VR_i at matched VR . Note that thermal fields were measured for all six conditions but PIV was used to measure all but the first condition ($VR_i = 0.24$, $VR_c = 0.2$, and $VR = 0.83$).

Measurement Techniques. Thermal and velocity fields were measured at selected planes within and downstream of the hole. Figure 4 shows the locations of the measurement planes used in this study. Both thermal and velocity field measurements were performed at the three $y-z$ planes at $x/d = 0$ and 5. In-hole thermal fields were measured at the $y-z$ plane at $x/d = -2$ extending down into the diffuser. In-hole velocity fields were measured at an in-hole plane that was normal to the direction of injection and intersected the upstream edge of the hole breakout. The velocity

Table 2 Test matrix for this study

VR _i	VR _c	VR	Thermal fields	PIV
0.24	0.2	0.83	Yes	No
0.24	0.4	1.67	Yes	Yes
0.36	0.4	1.11	Yes	Yes
0.36	0.6	1.67	Yes	Yes
0.71	0.4	0.56	Yes	Yes
0.71	0.6	0.83	Yes	Yes

**Fig. 4 Location of measurement planes for thermal and velocity field measurements**

fields were measured at a different in-hole plane than the thermal fields to better observe vortical structures in the jet.

Thermal Fields. Thermal fields were measured above the wall and within the diffuser of the film cooling holes using a Type E microthermocouple probe with a wire diameter of $50\text{ }\mu\text{m}$ or a hole diameter of 0.013. A density ratio of $DR = 1.2$ was achieved by setting the mainstream temperature to $T_\infty = 310\text{ K}$ and the coolant temperature to $T_j = 258\text{ K}$. While this density ratio was lower than the typical engine condition $DR \approx 2.0$, the results of Ref. [6] showed that the impact of internal crossflow on the near-hole jet profile was preserved between $DR = 1.2$ and 1.8 when inlet velocity ratio, VR_i , was held constant. That result is a strong indication that the near-hole thermal and velocity fields are not strongly dependent on DR . The probe and the coolant and mainstream thermocouples were calibrated from 254 to 313 K using a bath filled with propylene glycol and water mixture with a reported accuracy of $\pm 0.1\text{ K}$. The calibration uncertainty was estimated to be $\delta T = \pm 0.21\text{ K}$ based on the calibration repeatability. This estimated uncertainty was confirmed by moving the probe into the mainstream and down into the film cooling hole to confirm that the temperatures measured by the probe were within $\pm 0.22\text{ K}$ of the mainstream and coolant temperature measurements, respectively.

The thermal field probe was traversed within the test section using an assembly of three Zaber model T-LSR traverses with a stated positional accuracy of $\pm 15\text{ }\mu\text{m}$. The probe was located on the test surface using a mark made at the centerline of the hole. It was estimated that the probe could be located accurately to within $\pm 0.05d$ in the lateral and streamwise directions and $\pm 0.025d$ in the wall-normal direction. The probe was moved automatically through the measurement plane according to a predetermined grid. At each location, the temperature of the probe was sampled at a rate of 250 Hz over a period of 3 s in order to determine the mean temperature as an average of 750 measurements. Each profile was composed of about 320 measurement points not including repeats. The temperature fields reported in this study were normalized using the mainstream and jet temperatures

$$\theta \equiv \frac{T_\infty - T_{\text{probe}}}{T_\infty - T_j} \quad (2)$$

The test-to-test repeatability of the thermal field measurement is shown in Fig. 5 for $VR_i = 0.24$, $VR = 0.83$, $x/d = 0$, and $z/d = 0.33$ (which is at the location of peak lateral temperature). The

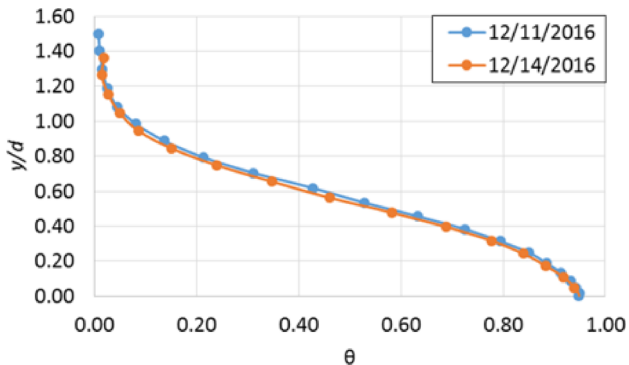


Fig. 5 Repeatability of the thermal field measurement for $VR_i = 0.24$, $VR_c = 0.83$, $x/d = 0$, and $z/d = -0.33$

uncertainty in the measurement was primarily a result of the strong turbulent fluctuations and sharp thermal gradients within the shear layer of the jet. Precision uncertainty in the shear layer was within $\delta\theta_p = \pm 0.05$ while in the jet core and mainstream, it was typically $\delta\theta_p = \pm 0.005$. Bias uncertainty was low due to the thermocouples sharing a common calibration standard and was estimated to be $\delta\theta_b = \pm 0.004$.

Particle Image Velocimetry. A PIV system was used to observe the flow structures within and near the film cooling holes. A Litron Lasers Model No. NANO L135-15 PIV dual ND:YAG laser was pulsed in coordination with a TSI Powerview Plus charged coupled device camera with a pixel resolution of 1600×1200 . A telephoto lens with a focal length of 180 mm and a maximum aperture of $f/3.5$ was used to view the measurement planes. A small mirror was mounted far downstream of the film cooling holes and was located on either the floor or ceiling of the test section to provide optical access for the camera.

An oil droplet generator provided atomized olive oil to seed the flow. The mean diameter of the oil droplets was between 0.5 and 1.0 μm , resulting in a Stokes number of up to 0.008 for the maximum expected velocity. For the Stokes number < 0.01 , seed particles are expected to resolve turbulent frequencies of at least 10 kHz [17]. For the $x/d = 0$ and 5 measurement planes, the seed was introduced to the recirculating tunnel for long enough to ensure that both the mainstream and coolant were seeded evenly. Due to concerns about seed performance at low temperatures, the PIV experiments were run at a density ratio of $DR = 1.0$. Because the density ratio impacts the mainstream-coolant interaction, it is not expected that the lower density ratio will impact in-hole flow field measurements where there is a minimal interaction between the mainstream and coolant. For the $x/d = 0$ and 5 locations, the lower density ratio may have reduced the strength of the observed counter-rotating pair but was certainly not responsible for the asymmetry and lateral location of that vortex pair. The laser pulses for the experiments were set to be 13 μs apart to permit sufficient time for tracking particle movement while not losing too great a percentage of particles through the plane. It was estimated that particles at the mainstream velocity would pass through the 1.1 mm thick laser sheet in 40 μs , resulting in roughly 68% particle retention from frame to frame.

For each test condition, 5000 image pairs were captured at a rate of 5 Hz. The image pairs were processed using PIVLAB, which is an open-source MATLAB application. The images were preprocessed using a high-pass filter to remove background noise and intensity capping to reduce the influence of brighter particles. The processing was performed using four passes using interrogation windows of 64, 32, 16, and 16 pixels per side with 50% overlap. Spurious vectors were removed with postprocessing filtering. For the measurement planes in which the mainstream flow could be viewed at $x/d = 0$ and 5, a correction was applied to account for

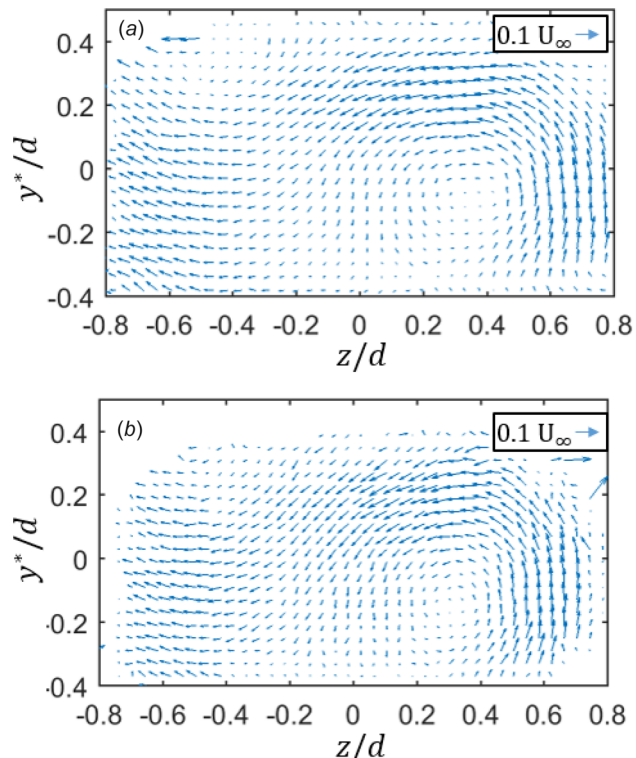


Fig. 6 Repeatability of in-hole PIV measurements for $VR_i = 0.71$ and $VR_c = 0.56$; (a) and (b) are from different experiments

the slight tilt of the camera relative to the plane to remove the bias errors from the mainstream flow.

The test-to-test repeatability of the measurement is shown by the vector field plotted in Fig. 6 for $VR_i = 0.71$, $VR_c = 0.4$, and $VR = 0.56$ for the in-hole plane normal to the direction of injection. The two vector fields are qualitatively similar in that they show the same vortical pattern. The velocity magnitudes were repeatable to within $\delta V = \pm 0.37 \text{ m/s}$, which was $\pm 27\%$ of the average in-plane velocity magnitude and $\pm 1.5\%$ of U_∞ . The velocity directions were repeatable to within $\delta\varphi = \pm 8 \text{ deg}$. Therefore, the PIV data presented here are useful to show the flow structures within the jet, which is the aim of this study.

Results and Discussion

Thermal and velocity fields were measured for a standard axial laidback fan-shaped film cooling hole at varying locations, cross-flow velocities, and injection rates. The objective of these measurements was to provide insight into the flow physics governing the impact of internal crossflow on film cooling performance—both within and immediately downstream of the shaped hole diffuser.

In-Hole Measurements. The impact of internal crossflow on film cooling effectiveness begins at the inlet of the hole. The internal flow is expected to separate on the windward side of the hole inlet as it enters the hole so that the bulk of the coolant enters the hole on the leeward side of the hole. Previous computational studies [4,13] have predicted that a strong swirling flow is initiated at the inlet of the hole, resulting in coolant biasing toward one side of the diffuser. Previous experimental studies have shown that for laidback fan-shaped holes, the coolant tends to bias toward the windward side of the diffuser relative to the internal crossflow for both the 7-7-7 holes previously tested in this laboratory [6] and for the wider angle laidback fan-shaped holes of Gritsch et al. [3]. To produce such a bias, the coolant would have to complete

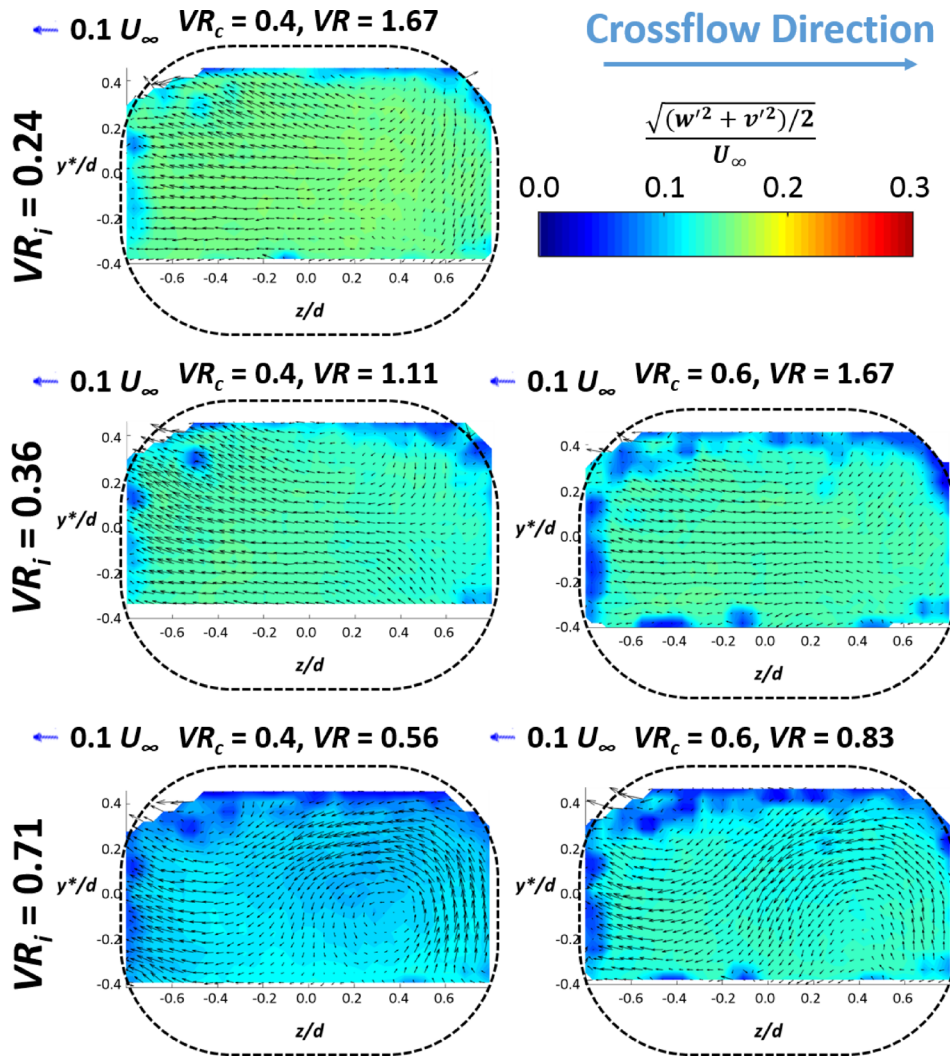


Fig. 7 Vector plots of in-hole mean velocity for all conditions tested overlaid on contours of in-plane turbulence intensity

roughly a half-turn before it exits the hole. McClintic et al. [6] showed that the severity of the biasing was a function of the inlet velocity ratio and was most severely biased toward the windward side of the diffuser at $VR_i = 0.36$.

A PIV system was used to observe the velocity field in the plane normal to the axis of the metering hole and coincident with the upstream edge of the hole breakout as shown in Fig. 4. Figure 7 shows vector plots for each flow condition tested in the in-hole plane overlaid onto the calculated in-plane turbulence intensity. The dashed line around each plot indicates the location of the walls of the hole. The coordinate y^* is the in-plane vertical direction and $y^* = 0$ at the intersection of the metering hole axis and the measurement plane. Each row of plots in Fig. 7 is at a constant inlet velocity ratio. For the greatest inlet velocity ratio tested, $VR_i = 0.71$, a remnant of the swirling flow was observed on the leeward side of the hole in the measurement plane. On the windward side of the hole, the PIV captured the spanwise component of the bulk flow of the jet within the diffuser. The coolant on that side of the jet moved toward the windward side of the hole which is consistent with the observed direction of biasing in the film cooling effectiveness measurements of Ref. [6]. At the lower inlet velocity ratios, $VR_i = 0.24$ and 0.36 , no evidence of swirling flow was observed as the bulk of the flow was directed toward the windward side of the hole. For all conditions, the fluctuating velocities were nearly constant throughout the measurement plane

and were greater at lower inlet velocity ratios (VR_i) and greater injection rates (VR).

The flow fields presented in Fig. 7 provide a number of interesting insights into the nature of the flow within the hole. First, the flow structures within the hole appear to scale with the inlet velocity ratio. This result agrees with the conclusions of Ref. [6], who showed that the severity of the biasing in the diffuser scaled with VR_i . Also, the bulk movement of the coolant toward the windward side of the diffuser, especially at $VR_i = 0.24$ and 0.36 , shows the coolant diffusing in only one direction, which is consistent with the direction of bias observed in Ref. [6]. The presence of tangential swirling flow at $VR_i = 0.71$ represents an experimental confirmation of the computational predictions of Saumweber and Schulz [4] and Kohli and Thole [13]. The absence of swirling flow at $VR_i = 0.24$ and 0.36 does not necessarily conflict with those predictions but suggests that the strongest swirling flow occurs in the cylindrical metering section of the hole and is attenuated as it moves down the hole and enters the diffuser. Note that [13] predicted that a reduction in crossflow velocity reduced the strength of the in-hole swirl which is consistent with these measurements. Furthermore, the computed pathlines in Ref. [13] appear to show a strong swirl at the inlet of the hole that attenuates as it passes through the hole. The magnitude of the swirling flow for $VR_i = 0.71$ was on the order of $0.1U_\infty$ (note that the uncertainty in this magnitude was estimated to be $\delta V/V = \pm 30\%$).

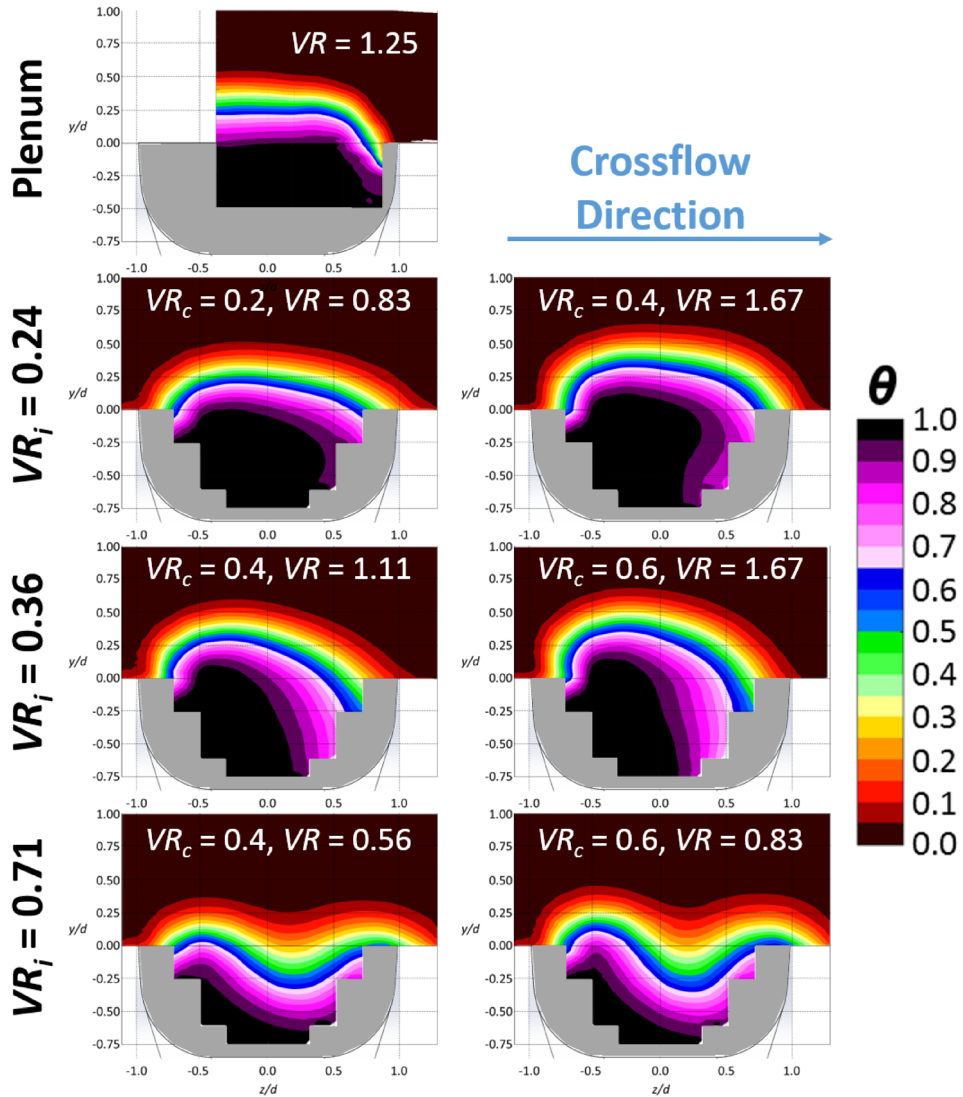


Fig. 8 Contours of normalized temperature in the y - z plane at $x/d = -2$ for all conditions tested

A simple approximation was used to calculate the mean swirling velocity upstream of the measurement plane

$$\bar{U}_s \equiv \frac{d\Delta\varphi}{L^*} \bar{U}_j \quad (3)$$

where U_s is the swirling (tangential) velocity, L^* is the distance from the inlet of the hole to the measurement plane along the hole axis and is equal to $5.13d$, and $\Delta\varphi$ is the total rotational angle traversed by the bulk flow of coolant starting at the leeward side of the hole inlet. For $VR_i = 0.36$ where biasing toward the windward side was maximum, $\Delta\varphi = \pi$, resulting in $U_s/U_j \approx 0.61$ for $VR = 1.11$ or $U_s/U_\infty \approx 0.68$, which is substantially greater than the secondary flow velocities observed in the measurement plane for any flow condition. The computational prediction of Saumweber and Schulz [4] predicted $U_s \approx 100 \text{ m/s}$ $2d$ into the cylindrical section of the hole for $VR_i = 1.3$, resulting in $U_s/U_\infty \approx 0.74$, which is consistent with the predicted value for this geometry.

In-hole thermal fields were also measured at $x/d = -2$ as indicated by Fig. 4. Note that this plane is different than the measurement plane for the PIV. Kohli and Thole [13] predicted that laidback fan-shaped holes fed by an internal crossflow had increased ingestion of mainstream air into the diffuser relative to

a plenum-fed hole. Figure 8 shows the in-hole thermal fields for all conditions tested and for a baseline plenum-fed hole at $VR = 1.25$. Again, each row of the figure is at a different inlet velocity ratio and the shape beneath each contour plot represents the shape of the diffuser at $x/d = -2$. The grayed out regions in the hole were regions in which the probe was not traversed. Like the in-hole velocity fields, the in-hole thermal fields largely scaled with the inlet velocity ratio, confirming again that the impact of internal crossflow on film cooling performance scales with VR_i . The thermal field plots also provide evidence for the existence of a swirling flow that caused biasing within the diffuser. The plenum-fed hole at the top of the figure has a symmetric in-hole temperature profile. The predictions of Oliver et al. [11] for the same geometry and injection rate suggest that the bulk of the flow exited the plenum-fed hole on the upstream side of the hole relative to the mainstream. At an inlet velocity ratio of $VR_i = 0.24$, the core of the jet was located toward the upper-windward side of the diffuser relative to the crossflow direction. As the inlet velocity ratio increased to $VR_i = 0.36$ and 0.71 , the core of the jet moved in a counter-clockwise direction. This apparent rotation of the jet core strongly indicates the existence of rotational flow in the metering section of the hole.

For the crossflow-fed conditions, Fig. 8 shows that there was substantial ingestion of mainstream air into the diffuser. Ingestion

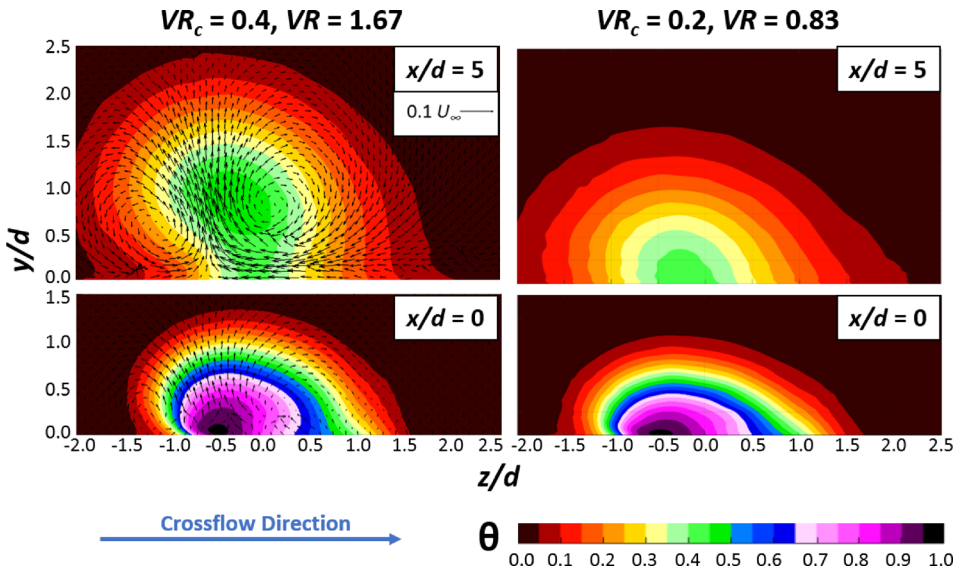


Fig. 9 Vector plots of mean velocity overlaid on contours of normalized mean temperature for $VR_i = 0.24$

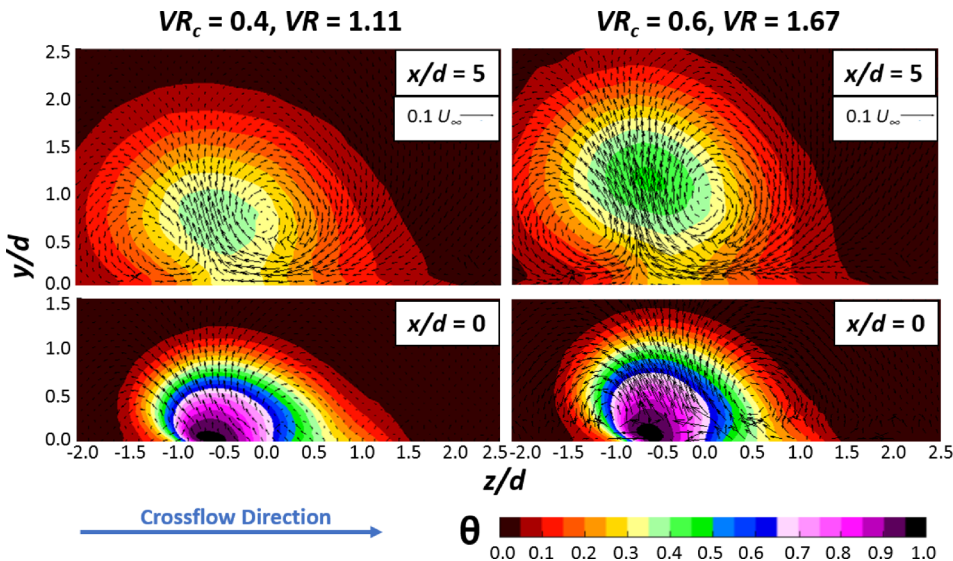


Fig. 10 Vector plots of mean velocity overlaid on contours of normalized mean temperature for $VR_i = 0.36$

is undesirable because it allows hot gasses to impact the surface of the hole and increases mixing of the mainstream and coolant in the hole such that it exits the hole at $\theta < 1$ and reduces the effectiveness downstream. At $VR_i = 0.24$, the mainstream air primarily ingested into the leeward side of the hole or on the side to which the coolant did not bias. As the inlet velocity ratio increased to $VR_i = 0.36$, the ingestion became more severe, such that it affected roughly half of the diffuser area. As VR_i increased further to 0.71, the coolant biased toward the bottom of the diffuser, allowing ingestion into the top center of the hole. Interestingly, the velocity fields presented in Fig. 7 show a downward movement of coolant in spanwise locations that corresponded to where ingestion occurred. At $VR_i = 0.24$ and 0.36, the velocity fields show a downward movement of the coolant at the upper leeward side of the hole that corresponded with ingestion into that region. Additionally, at $VR_i = 0.71$, the swirling flow has a downward trajectory in the top-center of the hole that corresponded with the ingestion into the top of the hole as shown in the thermal field

contours. This agreement between the thermal and velocity fields shows that not only did the secondary flow within the hole encourage coolant to bias within the diffuser but also it actively contributed to ingestion of mainstream gas.

Downstream Measurements. Previous studies showed that a counter-rotating vortex pair formed downstream of plenum-fed 7-7 holes and contributed to the dispersal of the jet as it moved downstream [11,12]. Saumweber and Schulz [4] computationally predicted that internal crossflow caused an asymmetric counter rotating vortex pair that greatly increased the dispersion of the coolant away from the surface. In this study, velocity and temperature fields were measured at $x/d = 0$ and 5 to investigate the impact of internal crossflow on these vortical structures and on the dispersal of the coolant above the surface. Figures 9–11 show vector plots of tangential velocity overlaid on contours of θ for $VR_i = 0.24, 0.36$, and 0.71, respectively. Note that while the pitch

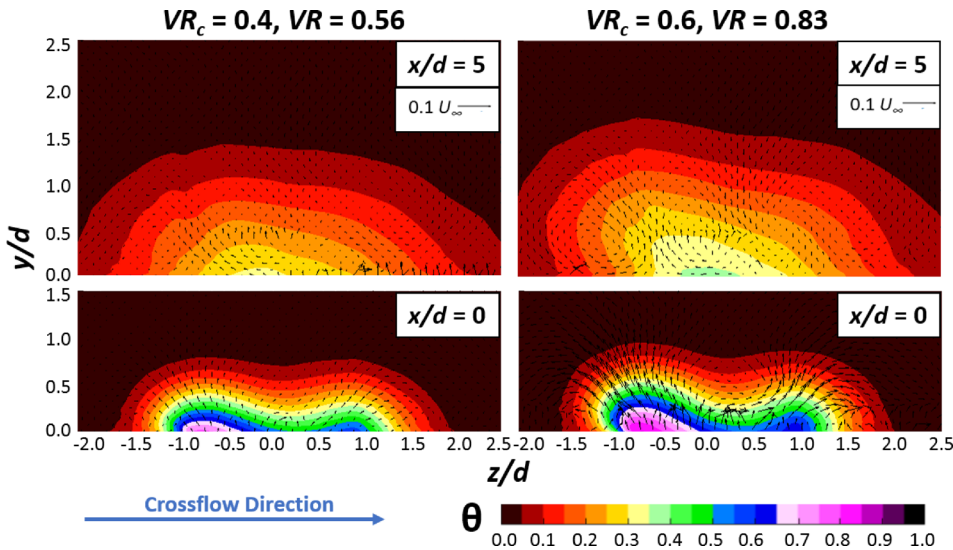


Fig. 11 Vector plots of mean velocity overlaid on contours of normalized mean temperature for $VR_i = 0.71$

spacing of the holes was $p/d = 6$, data are displayed only for $z/d = -2.0$ to 2.5 and $z/d = 0$ is the geometric centerline of the hole.

Unlike the in-hole temperature and velocity fields, the behavior of the downstream jets did not scale with the inlet velocity ratio but were noticeably impacted by the internal crossflow. At $VR_i = 0.24$, shown in Fig. 9, there was a substantial difference in the thermal fields between $VR = 0.83$ and 1.67 , especially at $x/d = 5$. The higher injection rate caused the jet core to lift off of the wall by $x/d = 5$ while the jet stayed well-attached at $VR = 0.83$. Evidence of an asymmetric counter-rotating vortex pair was observed for $VR = 1.67$. The vortex on the right side of the jet (on the leeward side relative to the crossflow direction) was higher above the wall than the vortex on the windward or left side. The asymmetrical vortices moved the jet core upward and in the negative z/d direction. Previously, [6] observed that the peak effectiveness at the wall had lateral movement as far downstream of the holes as $x/d = 30$, which was likely a result of this asymmetrical vortex pair.

Similar flow structures were observed at $VR_i = 0.36$, as shown in Fig. 10. For both $VR = 1.11$ and 1.67 , the leeward vortex was further from the wall than the windward vortex and the jet core moved up and in the negative z/d direction. Again, the two injection rates exhibited different degrees of separation. The core of the jet was colder for $VR = 1.67$, presumably because there was a greater mass flow rate of the coolant but for both conditions, the jet core had detached from the wall by $x/d = 5$. Recall that the maximum biasing occurred at $VR_i = 0.36$. It is likely because the jet was so strongly biased in the diffuser, as shown previously in Fig. 8, the jets at $VR_i = 0.36$ were considerably under-diffused and more prone to detaching from the wall. This effect can be observed by comparing the two cases with $VR = 1.67$ in Figs. 9 and 10. While both jet cores were detached from the wall, at $VR_i = 0.24$, the temperature under the core and near the wall was much colder than for $VR_i = 0.36$, indicating a greater degree of jet detachment for the greater inlet velocity ratio. Figures 9 and 10 also show the near-wall temperature decreasing for $VR_c = 0.4$ as VR increased from 1.11 to 1.67 . This occurred due to reduced jet detachment at $VR_i = 0.24$ and is consistent with the result of Ref. [6], who showed an increase in effectiveness from $VR = 1.11$ to 1.67 for $VR_c = 0.4$.

The flow and thermal fields for $VR_i = 0.71$ behaved much differently than for the lower inlet velocity ratios, as shown in Fig. 11. Because the two conditions tested were at lower injection rates of $VR = 0.56$ and 0.83 , the jets did not detach from the wall.

Furthermore, because the core of the jet was biased toward the bottom of the diffuser, the jets had increased lateral spreading. Previously, Schroeder and Thole [12] showed that plenum-fed holes had a weaker counter-rotating vortex pair at lower injection rates. A similar result was observed for $VR_i = 0.71$, especially at $VR = 0.56$ where the vortex pair could not be observed at all. At $VR = 0.83$ and $VR_i = 0.71$, the windward vortex was clearly defined at $x/d = 5$ while the leeward vortex was barely discernible. While the lower injection rate certainly contributed to the weakening of the vortices, the lateral spreading of the jet likely contributed to weaken the vortices as well. Because the jet exited the hole on the bottom of the diffuser, it presented less of a barrier to the mainstream flow. This difference can be observed by comparing the thermal fields for $VR = 0.83$ for $VR_i = 0.71$ and 0.24 . At $VR_i = 0.71$, the jet had a warmer core and greater lateral spreading than the jet at $VR_i = 0.24$ at $x/d = 5$. Interestingly, both jets had similar vertical dispersion to about $y/d = 1.5$. While neither jet detached from the wall, it is reasonable to hypothesize that $VR_i = 0.71$ would detach at a higher injection rate than $VR_i = 0.24$ due to the differences in diffuser performance.

Conclusions

Previous studies have shown that internal crossflow reduces the film cooling effectiveness of laidback fanshaped film cooling holes by causing the coolant to bias toward one side of the diffuser. This study measured the flow and temperature fields for a standard shaped hole to investigate the flow physics and dispersion of the coolant that cause the observed degradation in effectiveness. Inlet velocity ratios of $VR_i = 0.24, 0.36$, and 0.71 were tested. $VR_i = 0.36$ had been previously found to correspond to maximum biasing within the diffuser for the film hole geometry of interest. The important conclusions of this study are:

- It was experimentally confirmed that a swirling flow within the metering hole causes the coolant to bias within the diffuser. The remnants of this swirling flow were observed at $VR_i = 0.71$ at much weaker swirl velocities than required to produce the observed bias, indicating the swirl was substantially attenuated as it passed through the hole. In-hole thermal field measurements showed the jet core rotating from top center around to the bottom of the diffuser as VR_i was increased.
- In-hole thermal field measurements also showed substantial ingestion of mainstream air into the diffuser. Because

ingestion increases mixing with the mainstream and increases the temperature of the coolant before it exits the hole, it is an undesirable phenomenon. In-hole velocity field measurements agreed well with the thermal field measurements showing that the in-hole flow structures contributed toward the ingestion of mainstream air.

- An asymmetric counter-rotating vortex pair was observed for $VR_i = 0.24$ and 0.36 . The vortices lifted the core of the coolant jet vertically away from the surface and laterally away from the hole centerline, transporting coolant away from the wall and moving the jet laterally.
- Downstream thermal fields at $VR = 1.67$ showed that as biasing increased from $VR_i = 0.24\text{--}0.36$, the jet detachment from the wall also increased. Because the diffuser was less effective at reducing the relative momentum of the jet with increased biasing, those conditions were more susceptible to detachment.

The results of this study provide valuable insight into the behavior of film cooling jets from axial shaped holes fed by an internal crossflow. They also confirm, to an extent, previous computational predictions and provide a useful standard against which to validate future computational work.

Acknowledgment

The authors are grateful for the continued financial and technical support from GE Aviation and GE Global Research.

Nomenclature

d	= film cooling hole diameter
DR	= density ratio ρ_c/ρ_∞
f	= focal length
h	= heat transfer coefficient
H	= boundary layer shape factor
k	= thermal conductivity
L	= film cooling hole length
L^*	= length from hole inlet to in-hole PIV plane
L_m	= metering hole length
M	= blowing ratio $\rho_j U_j / \rho_\infty U_\infty$
Ma	= Mach number
p	= film cooling hole pitch
Re	= Reynolds number
T	= temperature
Tu	= turbulence intensity $\sqrt{u'^2}/\bar{U}$
U	= velocity
V	= velocity magnitude
v'	= fluctuating velocity in y^* direction
VR	= injection velocity ratio U_j/U_∞
VR_c	= crossflow velocity ratio U_c/U_∞
VR_i	= inlet velocity ratio U_i/U_j
w'	= fluctuating velocity in z direction
x	= streamwise coordinate measured from downstream edge of cooling hole
y	= wall-normal coordinate measured from the wall
y^*	= vertical coordinate for in-hole measurement plane
z	= spanwise coordinate

Greek Symbols

α	= cooling hole injection angle
β	= cooling hole lateral expansion angle

δ	= boundary layer thickness, uncertainty
δ^*	= boundary layer displacement thickness
η	= adiabatic effectiveness
θ	= normalized temperature, boundary layer momentum thickness
Λ_x	= turbulence integral length scale
ρ	= density
φ	= in-plane velocity direction angle
γ	= forward expansion angle

Subscripts

aw	= adiabatic wall
b	= bias uncertainty
c	= coolant, crossflow
d	= hole diameter
j	= coolant jet in metering section
p	= precision uncertainty
s	= swirling flow
∞	= mainstream
$-$	= mean

References

- [1] Bogard, D. G., and Thole, K. A., 2006, "Gas Turbine Film Cooling," *J. Propul. Power*, **22**(2), pp. 249–270.
- [2] Bunker, R. S., 2005, "A Review of Shaped Hole Turbine Film-Cooling Technology," *ASME J. Heat Transfer*, **127**(4), pp. 441–453.
- [3] Gritsch, M., Schulz, A., and Wittig, S., 2003, "Effect of Internal Coolant Crossflow on the Effectiveness of Shaped Film-Cooling Holes," *ASME J. Turbomach.*, **125**(3), pp. 547–554.
- [4] Saumweber, C., and Schulz, A., 2008, "Comparison of the Cooling Performance of Cylindrical and Fan-Shaped Cooling Holes With Special Emphasis on the Effect of Internal Coolant Cross-Flow," *ASME Paper No. GT2008-51036*.
- [5] Saumweber, C., and Schulz, A., 2012, "Effect of Geometry Variations on the Cooling Performance of Fan-Shaped Cooling Holes," *ASME J. Turbomach.*, **134**(6), p. 061008.
- [6] McClintic, J. W., Anderson, J. B., Bogard, D. G., Dyson, T. E., and Webster, Z. D., 2017, "Effect of Internal Crossflow Velocity on Film Cooling Effectiveness—Part I: Axial Shaped Holes," *ASME J. Turbomach.*, **140**(1), p. 011003.
- [7] Pietrzyk, J. R., Bogard, D. G., and Crawford, M. E., 1989, "Hydrodynamic Measurements of Jets in Crossflow for Gas Turbine Film Cooling Applications," *ASME J. Turbomach.*, **111**(2), pp. 139–145.
- [8] Pietrzyk, J. R., Bogard, D. G., and Crawford, M. E., 1989, "Effects of Density Ratios on the Hydrodynamics of Film Cooling," *ASME Paper No. 89-GT-175*.
- [9] Issakhanian, E., Elkins, C. J., and Eaton, J. K., 2012, "In-Hole and Mainflow Velocity Measurements of Low-Momentum Jets in Crossflow Emanating From Short Holes," *J. Exp. Fluids*, **53**(6), pp. 1765–1778.
- [10] Leylek, J. H., and Zerkle, R. D., 1994, "Discrete-Jet Film Cooling: A Comparison of Computational Results With Experiments," *ASME J. Turbomach.*, **116**(3), pp. 358–368.
- [11] Oliver, T. A., Anderson, J. B., Bogard, D. G., Moser, R. D., and Laskowski, G., 2017, "Implicit LES for Shaped-Hole Film Cooling Flow," *ASME Paper No. GT2017-63314*.
- [12] Schroeder, R. P., and Thole, K. A., 2016, "Effects of High Freestream Turbulence on Flowfields of Shaped Film Cooling Holes," *ASME J. Turbomach.*, **138**(9), p. 091001.
- [13] Kohli, A., and Thole, K. A., 1998, "Entrance Effects on Diffused Film-Cooling Holes," *ASME Paper No. 98-GT-402*.
- [14] Anderson, J. B., Wilkes, E. K., McClintic, J. W., and Bogard, D. G., 2016, "Effects of Freestream Mach Number, Reynolds Number, and Boundary Layer Thickness on Film Cooling Effectiveness of Shaped Holes," *ASME Paper No. GT2016-56152*.
- [15] Wilkes, E. K., Anderson, J. B., McClintic, J. W., and Bogard, D. G., 2016, "An Investigation of Turbine Film Cooling Effectiveness With Shaped Holes and Internal Cross-Flow With Varying Operational Parameters," *ASME Paper No. GT2016-56162*.
- [16] Schroeder, R. P., and Thole, K. A., 2014, "Adiabatic Effectiveness Measurements for a Baseline Shaped Film Cooling Hole," *ASME Paper No. GT2014-25992*.
- [17] Tavoularis, S., 2005, *Measurement in Fluid Mechanics*, Cambridge University Press, New York.